Die Attach and Thermal Cycling of Additively Manufactured Quad Flat No Lead Die Daisy Chain on Curved Alumina Substrate

Erik Busse[1], Mousa Al-Zanina[1], Abdullah Obeidat[1], Emuobosan Enakerakpo[1], WT Alshaibani[1], Stephen Gonya[1], Matthew Erdtmann[2], Adrian Pyke[2], Mark Poliks[1]
Binghamton University
4400 Vestal Parkway East
Binghamton, NY 13902 USA
Ph: 516-697-5594
Email: ebusse1@binghamton.edu

Abstract
Integration of electronic components into aerospace platforms offers the unique challenges of limited and constrained volumes. Utilizing non-planar surfaces allows for a drastic increase in the area available for electronics integration. Additive manufacturing (AM) can meet this need by working with a variety of substrate geometries to produce non-planar circuits capable of operating in harsh space environments.

Here we demonstrate the use of aerosol jet printing (AJP) and dispense printing to integrate passive traces of a daisy chain to a silicon-based quad flat no lead (QFN) die onto curved 96% purity alumina substrates. Adhesion of multiple material interfaces was tested to determine the compatibility of different components. AJP was used to fabricate all traces and bond pads using silver-based ink. Assembly was completed by depositing a conductive epoxy to attach the die. Samples were placed in an environmental chamber and cycled between –55°C and 125°C for 10 cycles as per MIL-STD-883, M1010, Condition B. Afterwards, the change in resistance was measured for all lines in the fabricated daisy chain.

All interfaces provided strong adhesion since the failure mode of most interfaces was adhesive failure and not cohesive failure between the deposited layers and substrate. The only interface which experienced consistent cohesive failure was the conductor on the dielectric pad. Despite the failure mode, this material was selected as the adhesive force was still acceptable. Two samples fabricated on convex and concave alumina substrates were subjected to thermal cycling to study the effect of temperature variation on the assembly, and the results found that no variance in the lines resistance exceeded a ±10% change in resistance. Overall, the devices performed well with changes in resistance being better mitigated by thicker conductive layers. The additive manufacturing techniques demonstrated in this work enhance the electronic industry by improving performance and reliability while simultaneously reducing the material cost and waste.

Key words
Additive manufacturing, passive electronic components, spaceborne electronic application, aerosol jet printing, curved ceramic.

I. Introduction
Aerospace applications have a long list of performance and material requirements due to the high stress nature of their environment. A common constraint from these platforms is that of volume and weight of the overall system. The heavier and bulkier the platform, the more fuel is required to launch. Current electronics are often found on large, flat, and planar circuit boards which require a large amount of dedicated space for integration. If we change the geometry of the substrate we integrate electronics with we can make use of previously unused space. Even just using a curved substrate can increase the surface area and allow for integration into new spaces. To fabricate devices onto the faces of non-planar substrates, we need to investigate what techniques are available to us.

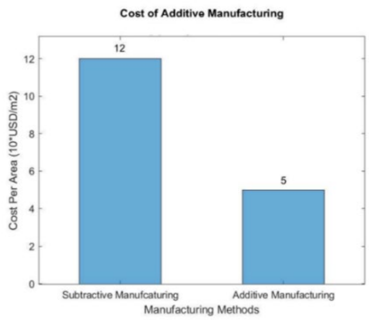

Figure 1: A summary of the work done by Dong et, al. to visualize the decrease in cost per surface area achieved by AM when compared to subtractive methods.

Additive Manufacturing (AM) techniques allow us to apply a variety of materials where they are required, as opposed to subtractive manufacturing which produces excessive material waste. As explored by Dong *et al.* in Figure 1, we can see that AM can decrease cost of electronic per surface area significantly [1].

One way AM is changing the way we think of electronics is by changing the way we fabricate substrates. Alumina or aluminum oxide is a very popular high temperature ceramic substrate owing its popularity to its mechanical and dielectric properties, as well as its thermal stability [2], [3], [4]. Printing ceramics using Digital Light Projection (DLP), photopolymer resins containing ceramic powders are cured [5], and allow for a variety of designs to be made with ease. However, printing substrates is only the first step, since we must also investigate fabrication techniques which are compatible with these non-planar substrates.

One such AM method is Aerosol Jet Printing (AJP). AJP is a contactless printing method which is compatible with a wide variety of materials, both conductive and dielectric. AJP is widely known for its relatively narrow achievable line widths, as low as 10 µm [6]. These narrow trace widths have shown that AM does more than just create sensors, but can also integrate silicon-based chips [7], [8], [9].

Paulsen *et al.* have demonstrated foundational work for AJP with non-planar substrates [10]. Passive components were printed to curved alumina to demonstrate the applications of AJP in aerospace platforms. By integrating into the *+Z* direction, the authors were able to integrate more electronics per planar surface area.

In this work, we explore how AM, and more specifically AJP and dispense printing, can be used to fabricate conductive traces on convex and concave substrates. Additionally, a silicon QFN die is integrated into the circuit to determine how effective this method is at integrating silicon-based die.

II. Methodology

A. Aerosol Jet Printing (AJP) and Dispense Printing

AJP is a contactless direct-write printing method which can utilize a variety of different material-based inks. Atomization begins with either a pneumatic pressure or ultrasonic frequency being applied to the ink where aerosolized particles are then taken away by a carrier gas. The aerosolized particles are then further filtered in the virtual impactor where an exhaust gas flow carries off less inert particles. Finally, the stream of particles is collimated once more by a coaxial sheath gas. The final jet of particles can achieve relatively narrow line widths (10 µm). An Optomec 500 Series AJP, as pictured in Figure 2, was used in this work for its compatibility with three-dimensional substrates.

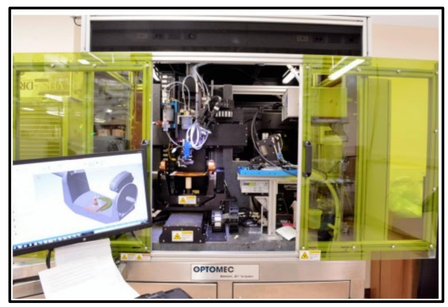

Figure 2: Optomec 500 Series AJP.

Many materials can be made compatible with the AJP leading to its versatility. In order for materials to be compatible with AJP, the viscosity must fall between 1–1000 cP [11].

Dispense printing requires contact with the substrate. Compared to AJP, dispense materials have far less constraints on material viscosity and particle sizes. To dispense material, we apply constant pneumatic pressure to the back of a syringe plunger. With these simple mechanics, we can work with a variety of different materials. Most importantly, dispensing techniques are often compatible with screen printable inks. These inks tend to have a higher viscosity, and because study involving screen printers is more mature, we have a large array of materials available to us. It should be noted dispense printing generally does not achieve as narrow a line width as AJP.

In this work the dispense printer will be used to fabricate an interposer. This interposer will be used to locally planarize an area on the substrate for the die to be integrated onto. The dielectric paste used to do this is DuPont QM44, a thick-film dielectric paste intended for high temperatures.

B. Materials Selection

The base of this work is the curved alumina substrate. The substrate used was a 96% purity alumina ceramic with a radius of curvature of two inches along one axis.

Silicon die cannot be directly mounted onto curved substrates without some planarized area. DuPont QM44 was chosen for this interposer for its adhesion to alumina substrates and its high temperature compatibility. Although this circuit was not designed for high temperatures, the good adhesion and ease of processing this ink offers make it a strong candidate for the interposer.

For this material, the dispense printer is the more appropriate deposition method, because the QM44 has a viscosity of around 80,000 to 120,000 cP, which is far too thick for the AJP [12]. Additionally, the dispenser can build thick layers of material with relatively fewer passes than the AJP. Given the 2-inch radius of curvature of the substrate, in order to fit the QFN die, the interposer requires an area of 9 mm × 9 mm and a thickness of 80 µm at its thickest point to obtain a flat surface.

The conductive element of this work, NovaCentrix Metalon® HPS-108AE1 silver-based nano flake ink, is intended for pneumatic atomization in the AJP with a viscosity of around 150 cP [13]. This ink was chosen for its relatively good adhesion to alumina and its ease of processing on the AJP.

Finally, to attach the die to the silver pads, a conductive, silver-based epoxy was used. EPO-TEK® H20E-PFC was dispensed onto all the pads before attaching the die. A silver-based epoxy was used as this circuit will only experience temperatures as high as 125°C, and the silver base of the epoxy allows it to be compatible with the chosen silver ink.

C. Trace Design and Simulation

Daisy chain and toolpath designs were all done in AutoCAD. The design for the daisy chain contained three pads per face and one at each corner and was intended to complement the internal daisy chain of the QFN die. After the toolpath was designed, the toolpath was ported into MasterCam 2019, where the toolpath was projected onto a model of the curved substrate, as seen in Figure 3. The toolpath is simulated in coordination with the models of the substrate, AJP nozzle, and substrate holster to determine if there are any collisions with the print head and substrate.

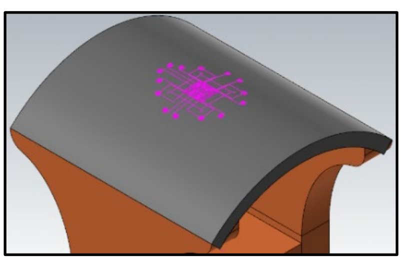

Figure 3: Daisy chain projected onto convex side of the simulated curved substrate.

The toolpath was simulated on the concave and convex side of the substrate. Following the simulations, a three-dimensional toolpath was extracted and loaded onto the Optomec 500 Series AJP. Two samples on each of the convex and concave sides were printed.

It should be noted the traces were printed without a heated platen, while QFN pads were printed with a platen temperature of 60°C. This is because the QFN pitch was the most critical element of this print, and so the individual layers were dried almost instantly.

D. Reliability Test

To determine the functionality of the devices, thermomechanical and thermoelectrical tests were conducted. All tests were carried out both before and after being thermally cycled. The thermal cycling schedule was based off MIL-STD-883, M1010, Condition B, in which the samples were cycled from -55 °C to 125 °C for 10 cycles.

First, a tensile adhesion test was carried out to test the adhesion of every interface present in this circuit, which includes silver to alumina, QM44 to alumina, and silver to QM44. Following this, a shear adhesion test was performed to determine the shear strength of the assembled die on the interposer and silver pads. All tests were performed again after samples underwent the thermal cycling schedule.

Next, resistance stability tests were performed by recording the resistance across each pad in the sample both before and after the thermal cycling schedule.

III. Results

A. Printability of Materials

Both QM44 and HPS-108AE1 inks were optimized before final prints took place. HPS-108AE1 was optimized to have a narrow line width while QM44 was optimized to have a wide and thick line.

The optimized QM44 had a line width and thickness of 143.0 ± 13.3 µm and 28.5 ± 2.4 µm respectively. The final optimized interposer had a thickness of 87.5 ± 4.8 µm, which met the 80 µm target. Above that, there was very little tolerance for printing over the target thickness, excessive pooling of dielectric resulted in cracks which severed traces after curing. Cracking is present in Figure 4, which was eliminated after optimization of the thickness.

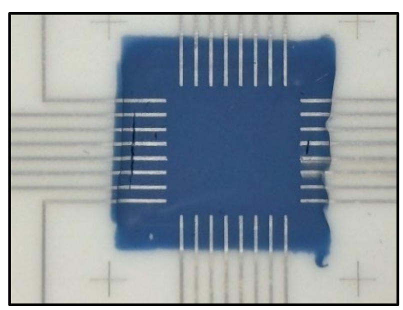

Figure 4: QM44 pad with silver lines printed. Improper optimization resulted in cracking as seen in the left side of the pad.

The optimized silver lines had a width and thickness of 53.0 ± 4.6 µm and 3.9 ± 0.4 µm, respectively. A trace width this

narrow was considered acceptable as the QFN has a pitch size of 650 µm. This thickness was achieved after only two layers, which is desirable because fewer layers required means fewer passes where errors can occur.
We can see examples of the final printed die in Figure 5. Looking at 5A and 5C we can see where optimization of line width becomes important as traces route the QFN to the test pads. Figure 5B shows sample S4 which was printed on the concave side as was sample S3. Similarly, Figure 5D shows sample S6 printed on the convex side, which is representative of sample S5 as well.

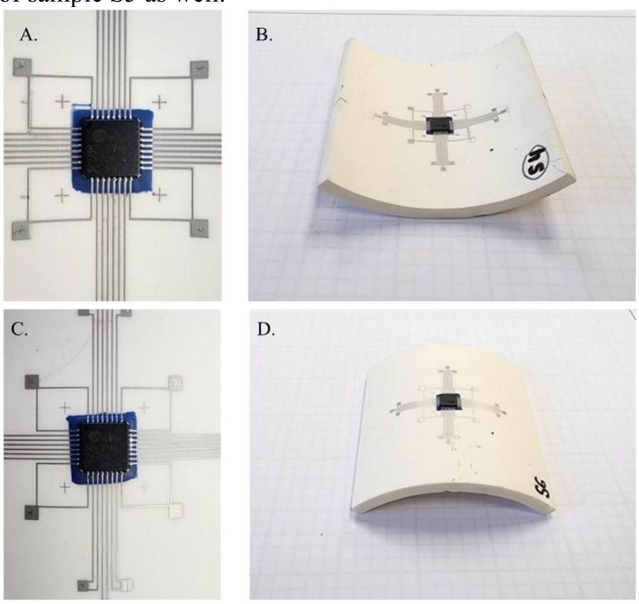

Figure 5: Images of (A and B) S4 with a close up of the attached die and (C and D) S6 with a close up of the attached die.

B. Tensile Adhesion

The tensile adhesive force of QM44 to alumina, silver to alumina, and silver to QM44 were evaluated before and after thermal cycling.
QM44 saw an average increase in its adhesion from 43.64 ± 2.92 kgF to 46.30 ± 2.34 kgF (Figure 6) for before and after thermal cycling, respectively, with the most common failure mode being an adhesive failure of the fitting's epoxy. Next, the silver was observed to have an adhesive force of 24.26 ± 12.64 kgF (Figure 7) before cycling and 18.97 ± 5.16 kgF after cycling, with the most common failure occurring invariably in the silver.

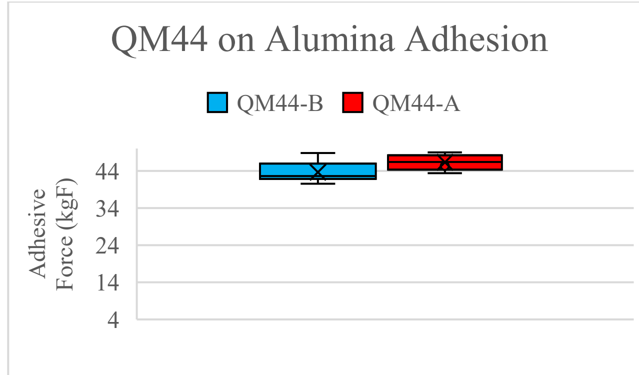

Figure 6: Tensile adhesion results of QM44 on 96% Alumina substrate both before (B) and after (A) thermal cycling.

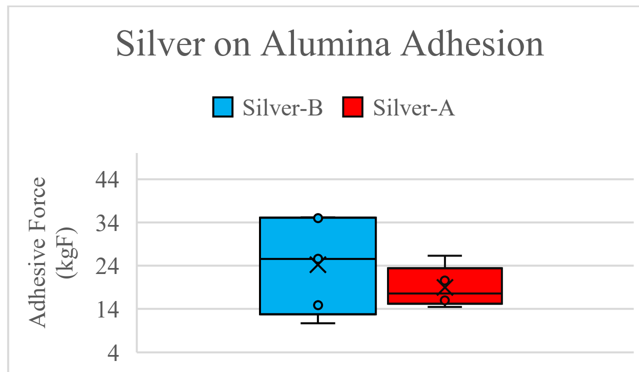

Figure 7: Tensile adhesion results of silver ink on 96% Alumina substrate both before (B) and after (A) thermal cycling.

The final stack of materials was tested with an alumina substrate, a QM44 pad, and silver pad on top. Here the adhesive force before and after thermal cycling was 7.37 ± 3.75 kgF and 18.08 ± 4.31 kgF (Figure 8), respectively, with failure occurring invariably in the silver in all cases.

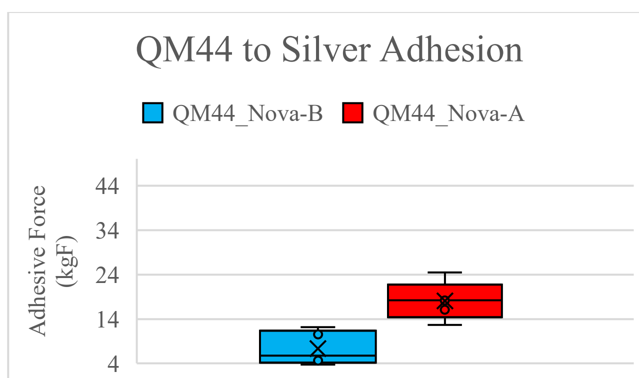

Figure 8: Tensile adhesion results of silver ink on QM44 interposer both before (B) and after (A) thermal cycling.

C. Shear Adhesion Test

After the QFN die was attached, a die shear test was preformed on the full stack of materials. The adhesive force was 18.70 ± 9.05 kgF and 16.69 ± 5.12 kgF (Figure 9) before and after thermally cycling, respectively, with the most common failure mode in both cases being a failure in the silver pads.

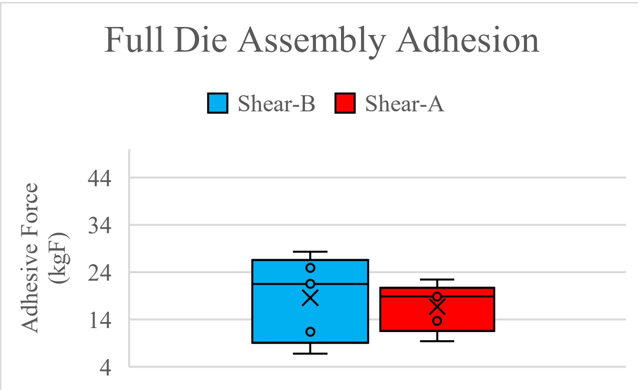

Figure 9: Shear adhesion results of full die assembly on 96% alumina both before (B) and after (A) thermal cycling.

D. Resistance Stability

The resistance across each pad of the printed daisy chain was tested before and after thermal cycling the full assembly. Two samples were printed on the concave side and two samples were printed on the convex side. Results are listed in Table 1. S4 and S6 had the highest and lowest changes in resistance of 7.40% and 0.64%, respectively.

Table 1: Resistance stability results

Sample	S3	S4	S5	S6
Average change in resistance (%)	2.76	7.40	5.31	0.64

IV. Discussion

A. Adhesion

The ability of materials to form strong adhesive bonds was evaluated first as this relationship is an early indication of material compatibility. QM44 has the largest adhesion value, however these are not necessarily representative of the QM44 to alumina bond. In all cases of QM44 samples, the failure was in the epoxy of the stud, which nominally has a maximum adhesive force of around 40–50 kgF. Although the values obtained for QM44 adhesion are not representative of this bond, we do know that its adhesive bond exceeds these values. Additionally, the slight increase in average adhesion seen from before to after thermal cycling similarly does not represent an observable increase in adhesion of the QM44 to alumina, as the predominant failure mode remained invariably in the stud epoxy.

The silver ink showed roughly half the adhesive force of QM44. Before thermal cycling, we see a large variance in the results from the silver ink, which decreased significantly after cycling. This decrease in variance can be best understood by looking at the densification of particles. This densification can be seen in Figure 10, not only in the decrease of the silver layer thickness, but also by the decrease in open spaces in the microstructure of the silver.

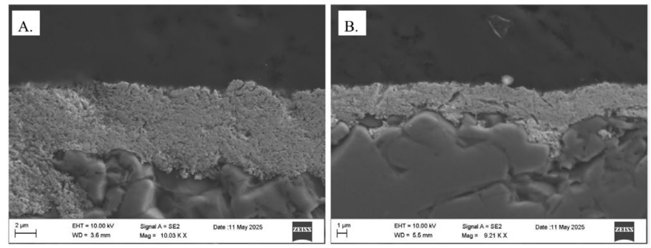

Figure 10: SEM image of the microstructure of silver ink (A) before and (A) after thermal cycling.

Shear adhesion has similar microstructural behavior for its changes in adhesive force. From what we can see in Figure 11, the thermal cycling had two effects that could have impacts on the adhesion, and both occur in the conductive epoxy. In Figure 11(A), the silver flakes of the conductive epoxy are less dense when compared to Figure 10(B). In Figure 11(B), although the flakes have densified, a CTE mismatch between the silver and QM44 has lead to fracturing in the dielectric layer. This fracturing provides an likely explanation in the loss of adhesion.

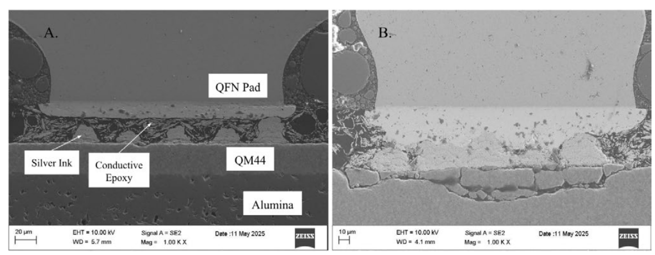

Figure 11: SEM image of the joint between QFN die and silver ink both (A) before and (B) after thermal cycling

B. Resistance Stability

The magnitudes in resistance changes vary greatly from sample to sample. S6 had the smallest change in resistance across any sample while S4 had the largest change in resistance. Each of these samples represent extremes in terms of layer thickness. S4 has a silver layer thicknesses of 9.239 ± 0.431 µm, while S6 has a silver layer thickness of 3.873 ± 0.366 µm.

Examining the microstructure, we can see physical reasons for the increase in resistance across all the samples. Although thicker layers indicate lower resistance, all conductive components are built of multiple layers. As seen in Figure 12, when comparing A and B we can see thermal cycling leads to separate silver layers beginning to delaminate. As these layers delaminate, resistance will be driven up. These pronounced layers are seen in the pads and not the traces because of the heated platen. Layers are dried almost instantly in the case of a heated platen, so each individual layer separates more easily.

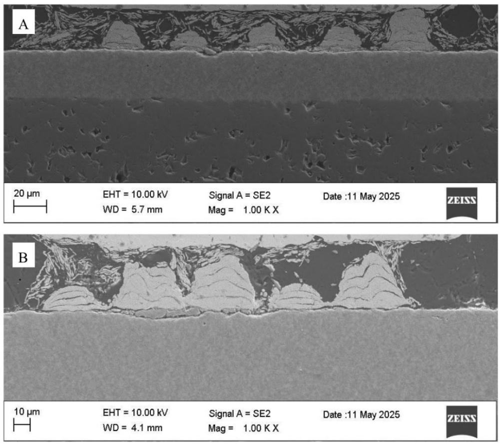

Figure 12: SEM image of individual lines of the silver ink pad (A) before and (B) after thermal cycling.

V. Conclusion

We have shown the ability of AJP to be compatible with not only printing on non-planar substrates but also its ability to integrate silicon die onto these complex substrates. The selected dielectric paste experienced some early printing issues with bubbling and excessive pooling. Following optimization of the printing parameters these issues were corrected.

Following printing optimization, the adhesion tests took place. When comparing adhesion tests before and after thermal cycling we can see that QM44 improves its adhesion after being cycled. This is seen as well in the case of QM44 to silver pads. Silver to the alumina surface had acceptable adhesion as well.

To look deeper into the reasons for the low adhesion force of the silver on dielectric, SEM was employed. In figures 11b and 12b we can see cracking occurring at the interface of the dielectric and silver pads. This cracking is brought on by a mismatch in the CTE of these two materials. Despite the silver ink providing a significant CTE mismatch, leading to weak adhesion force of the die on the interposer after thermal cycling, the complete package was able to perform after with less than a ±10% change in resistance.

In the future, a new conductor should be investigated to mitigate the CTE-related issues mentioned previously. Gold-based inks would complement the chosen dielectric ink by making all passive elements high-temperature compatible. Gold inks such as those studied by Alshatnawi *et al.* have very reliable adhesion to alumina and QM44 surfaces [14], [15], [16]. Additionally, new die will be integrated into these designs. Land grid array (LGA) and ball grid array (BGA) chip layouts will be integrated to display the ability of AM and specifically AJP as a method of integrating high density I/O chips onto nonplanar surfaces. Finally, we will look to study other high stress enviornemts to see the performance of theses structures when under high temperature and high humidity environments [17].

Acknowledgment

This material is based upon work supported by the National Aeronautics and Space Administration under Contract Number 80NSSC23PC014. Any opinions, findings, and conclusions or recommendations expressed in this material are those of the authors and do not necessarily reflect the views of the National Aeronautics and Space Administration.

This material is also based on research sponsored, in part, by Air Force Research Laboratory under agreement number FA8650-15-2-5401, as conducted through the flexible hybrid electronics manufacturing innovation institute, NextFlex. The U.S. Government is authorized to reproduce and distribute reprints for Governmental purposes notwithstanding any copyright notation thereon. The views and conclusions contained herein are those of the authors and should not be interpreted as necessarily representing the official policies or endorsements, either expressed or implied, of Air Force Research Laboratory or the U.S. Government.

References

[1] Y. Dong, C. Bao, and W. S. Kim, “Sustainable Additive Manufacturing of Printed Circuit Boards,” *Joule*, vol. 2, no. 4, pp. 579–582, Apr. 2018, doi: 10.1016/j.joule.2018.03.015.

[2] J. Kita, F. Schubert, F. Rettig, A. Engelbrecht, A. Groß, and R. Moos, “Ceramic Alumina Substrates for High-temperature Gas Sensors – Implications for Applicability,” *Procedia Engineering*, vol. 87, pp. 1505–1508, 2014, doi: 10.1016/j.proeng.2014.11.584.

[3] “96% Alumina Engineering Properties.” Accuratus, 2013.

[4] F. Miyashiro, N. Iwase, A. Tsuge, F. Ueno, M. Nakahashi, and T. Takahashi, “High thermal conductivity aluminum nitride ceramic substrates and packages,” *IEEE Transactions on Components, Hybrids, and Manufacturing Technology*, vol. 13, no. 2, pp. 313–319, 1990, doi: 10.1109/33.56163.

[5] J. Rauchenecker, “Development of aluminum nitride material systems suitable for additive manufacturing,” 2022.

[6] N. J. Wilkinson, M. A. A. Smith, R. W. Kay, and R. A. Harris, “A review of aerosol jet printing—a non-traditional hybrid process for micro-manufacturing,” *Int J Adv Manuf Technol*, vol. 105, no. 11, pp. 4599–4619, Dec. 2019, doi: 10.1007/s00170-019-03438-2.

[7] F. Alshatnawi *et al.*, “High Temperature Die Interconnection Approaches,” in *2022 IEEE 72nd Electronic Components and Technology Conference (ECTC)*, San Diego, CA, USA: IEEE, May 2022, pp. 1539–1545. doi: 10.1109/ECTC51906.2022.00245.

[8] A. S. Obeidat *et al.*, “Embedded RF Packaging Via Ceramic 3D Printing and Printed Electronics Additive Manufacturing,” in *2024 IEEE 74th Electronic Components and Technology Conference (ECTC)*, Denver, CO, USA: IEEE, May 2024, pp. 685–692. doi: 10.1109/ECTC51529.2024.00112.

[9] A. S. Obeidat *et al.*, “Effect of Thermal and Mechanical Stresses on Novel Microstrip Lines Printed on Flexible Substrates,” *IEEE Trans. Compon., Packag. Manufact. Technol.*, vol. 14, no. 8, pp. 1481–1492, Aug. 2024, doi: 10.1109/TCPMT.2024.3412740.

[10] J. A. Paulsen, M. Renn, K. Christenson, and R. Plourde, “Printing conformal electronics on 3D structures with Aerosol Jet technology,” in *2012 Future of Instrumentation International Workshop (FIIW) Proceedings*, IEEE, 2012, pp. 1–4.

[11] “AEROSOL JET 300 SERIES SYSTEMS.” Optomec, 2017.

[12] "QM44 Safty Data Sheet." DuPont.
[13] "Metalon® HPS-108AE1." NovaCentrix, 2016.
[14] F. Alshatnawi *et al.*, "Electrical and Mechanical Behavior of Aerosol Jet–Printed Gold on Alumina Substrate for High-Temperature Applications," *Adv Eng Mater*, vol. 25, no. 20, p. 2300439, Oct. 2023, doi: 10.1002/adem.202300439.
[15] D. Shaddock, C. Hoel, N. Stoffel, M. Poliks, and M. Alhendi, "Additively Manufactured Extreme Temperature Electronics Packaging," *International Symposium on Microelectronics*, vol. 2021, no. 1, pp. 000189–000194, Oct. 2021, doi: 10.4071/1085-8024-2021.1.000189.
[16] M. Al-Zanina *et al.*, "Mechanical and Electrical Evaluation of Materials for High Temperature Applications on Low CTE AlN Ceramic Substrates," in *2025 IEEE 75th Electronic Components and Technology Conference (ECTC)*, Dallas, TX, USA: IEEE, May 2025, pp. 1275–1281. doi: 10.1109/ECTC51687.2025.00219.
[17] B. Falola *et al.*, "Materials Evaluation for Flexible Hybrid Electronics: A Study on Conductive Inks and Die-Attach Materials," in *2025 IEEE 75th Electronic Components and Technology Conference (ECTC)*, Dallas, TX, USA: IEEE, May 2025, pp. 1864–1871. doi: 10.1109/ECTC51687.2025.00318.